PERGAMON

Journal of Structural Geology 22 (2000) 335–348

JOURNAL OF STRUCTURAL GEOLOGY

www.elsevier.nl/locate/jstrugeo

Synmetamorphic vein spacing distributions: characterisation and origin of a distribution of veins from NW Sardinia, Italy

G.D.H. Simpson*

IMP, Sonneggstr. 5, ETH, Zürich, CH-8092, Switzerland

Received 2 December 1998; accepted 19 October 1999

Abstract

The spatial distribution of a single generation of axial planar synmetamorphic veins exposed in greenschist facies rocks on NW Sardinia was investigated with the aim of gaining insight into the processes controlling the fracture spacing. The vein spacing distribution measured along linear profiles is non-uniform and approximately log-normal. Although the vein abundance and absolute vein spacing is strongly influenced by rock type, the vein spacing distribution is independent of rock type. Comparison of the observed data with synthetically generated fracture distributions indicates that the observed distribution can be reproduced by Kolmogorov fragmentation, but cannot be reproduced by a random, even-bisection or a fractal (Cantor Dust) process. These results are interpreted to indicate that the positions of fractures that become veins are interdependent. In an attempt to explain the interdependency of fracture positions, the perturbations of stress and fluid pressure associated with an isolated underpressured axial planar fracture were investigated. Simple calculations show that the fluid pressure drop inside a fracture coinciding with failure locally perturbs the stress and fluid pressure fields such that the surrounding rock, extending over a lateral extent equivalent to approximately two fracture lengths, is instantaneously driven into a critical stress state that satisfies the failure condition. Numerical simulations demonstrate that this process tends to localise the nucleation of subsequent fractures close to existing fractures. This mechanism can explain the existence of non-random or clustered fracture or vein spacing distributions forming by hydrofracture.

1. Introduction

Mineral-filled extension fractures or veins are common and regionally distributed in rocks metamorphosed to grades between the lower greenschist and granulite facies (Ramberg, 1961; Sawyer and Robin, 1986; Yardley, 1986; Fisher and Byrne, 1990; Yardley and Bottrell, 1992; Cartwright et al., 1994; Simpson, 1998). As with most fracture sets in natural materials, metamorphic veins are not evenly spaced (see Barton, 1995). In fact, the few studies that have characterised quantitatively the spatial distribution of metamorphic veins have shown that vein spacings follow power-law (fractal) distributions (Johnston, 1992; McCaffrey et al., 1993; Manning, 1994) or log-normal distributions (Fisher et al., 1995). These data indicate that vein sets display greater degrees of clustering than if veins were distributed purely randomly (see Manning, 1994; Fisher et al., 1995). While the distribution of veins is sometimes clearly related to lithology (e.g. Sawyer and Robin, 1986), clustered vein spacing distributions have also been observed within homogeneous rock types (McCaffrey et al., 1993). In this latter case, the presence of either a power-law or log-normal spacing distribution indicates that the position of veins (or fractures) are interdependent (Gillespie et al., 1993). Despite recognition of this interdependence, there has been little attempt to explain the spatial distribution of metamorphic veins explicitly in terms of likely physical processes (however see Segall, 1984; Blenkinsop, 1993).

This paper reports the results of a study of the vein spacing distribution within greenschist facies psammitic and pelitic metamorphic rocks exposed on NW Sardinia (Fig. 1), which was undertaken with the aim

* Present address: Département TAO, Ecole Normale Supérieure, 24 rue Lhomond, 75231 Paris Cedex 05, France.

E-mail address: simpson@geologie.ens.fr (G.D.H. Simpson).

0191-8141/00/$ - see front matter
PII: S0191-8141(99)00161-3

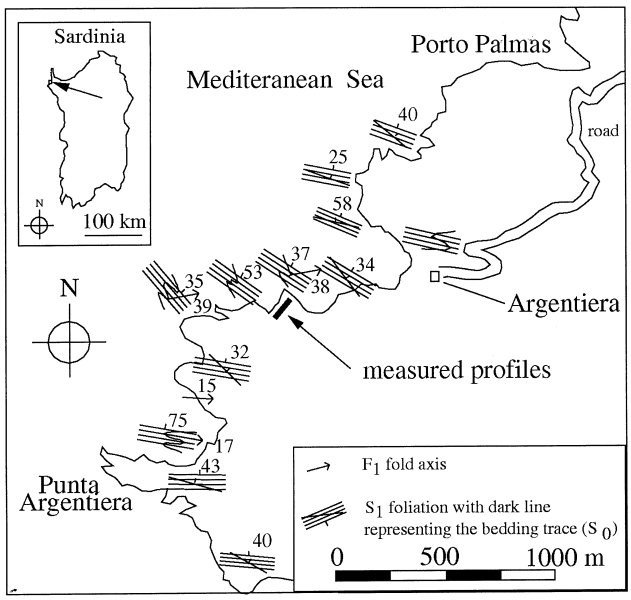

Fig. 1. Map (modified after Simpson, 1998) showing summary of (D_1) structures and the location of the measured profiles discussed in the text.

of gaining insight into the processes controlling the spacing distribution. The broad temporal and spatial relationship between deformation and dehydration reactions are described in a previous paper (Simpson, 1998; see also Carmignani et al., 1979, 1982; Franceschelli et al., 1990). The veins upon which this study is based occupy pure-extension fractures and form planar sets oriented parallel to axial planar foliations. Similar axial planar veins have been described from numerous metamorphic belts worldwide (Turner, 1941; Voll, 1960; Vidale, 1974; Yardley, 1975; Sawyer and Robin, 1986; Yardley and Bottrell, 1992). It is now generally accepted that axial planar veins form during deformation as the result of fluid pressure-induced hydrofracture of a low tensile strength foliation surface under low differential stresses (Kerrich, 1986; Gratier, 1987). This study demonstrates that the spacing of a single generation of axial planar veins displays non-random clustering, which is best described by a log-normal distribution. Simple theoretical consideration of the perturbations of fluid pressure and stress associated with existing fractures are investigated to determine the role of fluids in influencing the vein spacing distribution.

2. Metamorphic veins from NW Sardinia

2.1. General features of veins

Metamorphic veins are exposed in lower-greenschist facies Hercynian rocks on NW Sardinia (Simpson, 1998; see also Carmignani et al., 1979, 1982; Franceschelli et al., 1990). The sequence in which the veins are found (Fig. 1) is dominated by sandstones, phyllites and quartzites, which are interlayered on a scale of several centimetres to several tens of metres. The veins described within this work crop out in coastal exposures in the Argentiera region. The deformation of rocks in this area is dominated by penetrative D_1 structures which are overprinted by D_2 open buckling and the formation of a crenulation cleavage (Simpson, 1998).

The veins reported here are oriented parallel to a penetrative axial planar fabric (S_1) of regionally extensive tight (F_1) folds that formed during D_1 deformation. Such veins are weakly overprinted by D_2 macroscopic buckling (Fig. 2a) and a crenulation cleavage. The veins occur in planar sub-parallel sets, which cut across bedding contacts and show no fanning around F_1 fold hinges and no preference for fold hinges versus fold limbs (Fig. 2a). The occurrence of veins is controlled to some degree by the presence of lobe-and-cusp structures, which are developed at the contacts between competent psammitic units and relatively incompetent pelitic units (Fig. 2b). Many of the axial planar veins are boudinaged within the foliation surface (Fig. 2c). Together, these features indicate that the veins formed parallel to the (S_1) axial planar foliation (i.e. they were not rotated into this orientation by subsequent deformation) during the episode of deformation that formed the (F_1) folds. The axial planar veins have lengths of between 10 cm and approximately 20 m and thicknesses of between 1 mm and 10 cm. All veins narrow towards their terminations and have sharp, non-branching tips. The axial planar veins typically display no offset across their margins (Fig. 2d). Veins are filled dominantly with quartz, although carbonate, chlorite, muscovite and feldspar are also found. The vein minerals are identical to the minerals present in the adjacent rocks (but not in proportion). Original vein growth textures are seldom preserved due to recrystallisation of the original vein filling minerals. However, when original textures are preserved, euhedral grain terminations indicative of open space filling are observed (Fig. 2e).

2.2. Failure conditions

Observations (Fig. 2) indicate that the axial planar veins formed as open, fluid-filled fractures. Assuming that D_1 deformation is coaxial (a feature which is not quantitatively demonstrated but is consistent with field data) and that the penetrative S_1 axial planar fabric contains the X and Y axes of the finite strain ellipse, it follows that the stress and strain ellipsoids coincide and therefore that the mineral-filled axial planar fractures lie in a plane sub-perpendicular to σ_1 that

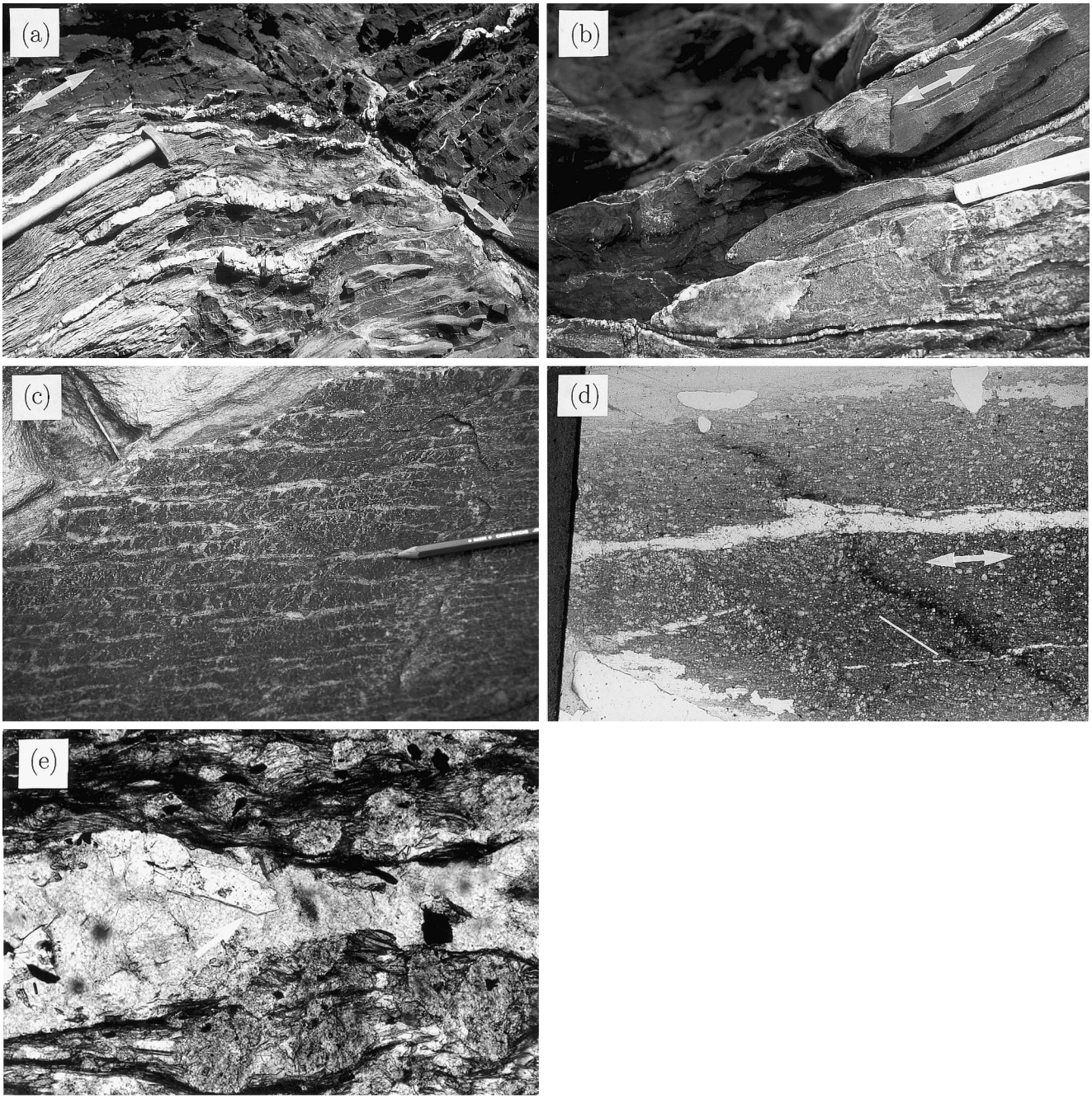

Fig. 2. (a) Set of quartz veins oriented parallel to the axial planar foliation (parallel to arrow in the upper left part of the photo) of a tight-isoclinal (F_1) fold. The folded bedding contact is marked by a row of white filled arrow-heads. Note that D_2 buckling and cleavage formation (the axial surface of which is approximately perpendicular to S_1 and is marked by an arrow in the right part of the photo) has a minor influence on the D_1 structures. (b) Lobe-and-cusp structures developed at the (F_1) folded bedding contact between an incompetent pelite (upper left) and a relatively competent psammite (lower right). Quartz veins cut through the cusp structures oriented parallel to the (S_1) axial planar surface (parallel to arrow). (c) View onto the surface of a carbonate-rich axial planar vein which was stretched parallel to the extension lineation (perpendicular to pencil) during D_1 deformation, broken and infilled by quartz. (d) Photograph of a thin section that shows an axial planar vein (parallel to arrow) cutting a bedding lamination (marked by a white bar) with no lateral displacement (field of view ca. 1×2 cm). Note the near absence of D_2 cleavage development. (e) Photomicrograph of an axial planar microfracture into which a quartz crystal with a euhedral termination has grown. The quartz crystal is interpreted to have grown into an open fluid-filled fracture during metamorphism (field of view ca. 2×3 mm).

contains σ_2 and σ_3. This inference is consistent both with the absence of shear displacement across the veins (Fig. 2d) and with the subsequent boudinage of the veins along the axial surface (Fig. 2c). The observed dilational displacements are thus inferred to have been driven by fluid pressure within the fractures. In the absence of reversals in the remote applied stresses, the conditions for the formation of axial planar fractures

are (e.g. Kerrich, 1986; Gratier, 1987):

$$p_f = \sigma_1 + T_s \quad (1)$$

and

$$(\sigma_1 - \sigma_3) < (T - T_s) \quad (2)$$

where p_f is the fluid pressure (assumed positive), σ_1 and σ_3 (both of which are assumed to be positive in compression) are the local maximum and minimum

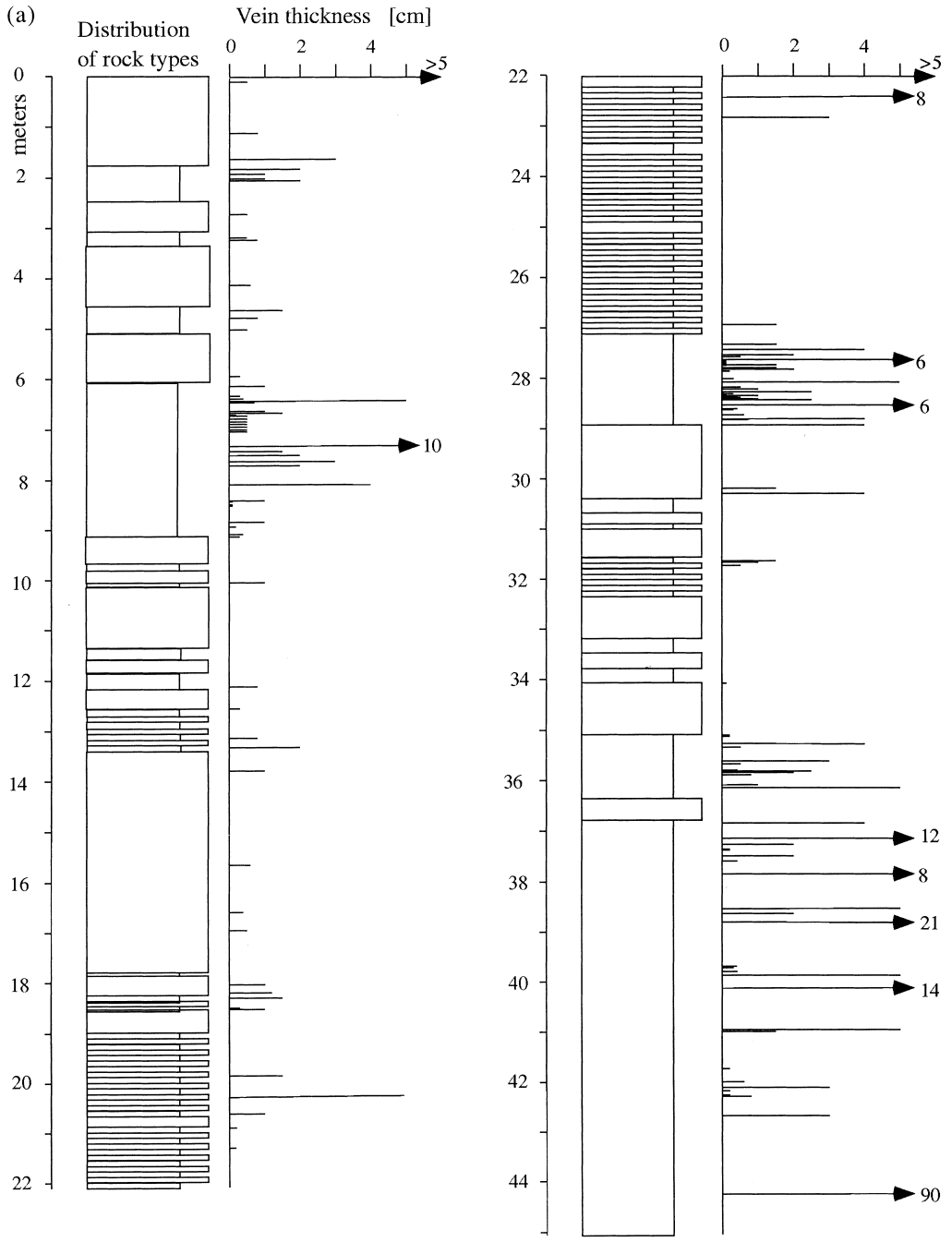

Fig. 3. Distribution and thickness of (D_1) axial planar veins (right hand column) and rock types (left hand column) in one-dimensional profiles oriented perpendicular to the strike of the veins and the (S_1) axial planar foliation. Veins thicker than 5 cm are indicated by an arrow and the vein thickness (in cm). Rock types are divided into pelite (narrow box) and psammite (wide box). (a) Continuous measured section (termed profile 1) located on the coast approximately 700 m west of Argentiera. The profile has an average of 8% volume veins with a mean vein spacing of 28 cm and a mean vein thickness of 25 mm (total number of veins 114). (b) Nine separate profiles (labelled A–I) measured in continuous, homogeneous pelitic or psammitic units from within 200 m of profile 1. The profiles are presented here in a combined column (total number of veins 200). The real boundaries between the different profiles coincide with the rock type changes in the combined column.

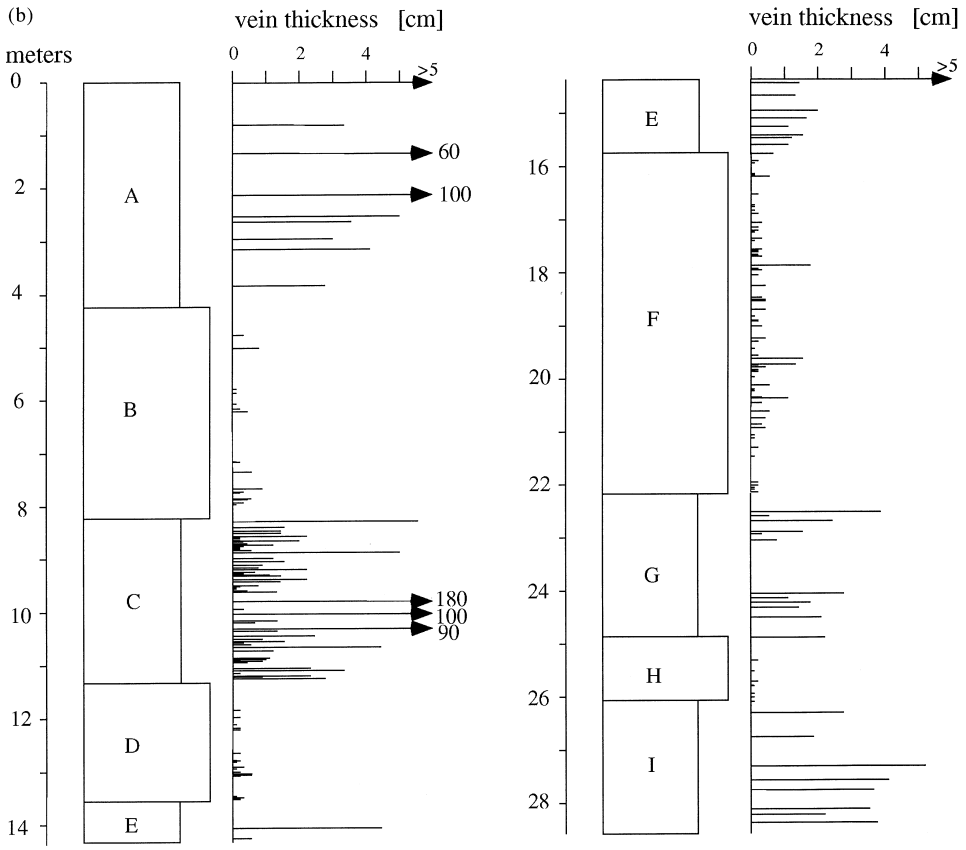

Fig. 3 (*continued*)

principal compressive stresses, T_s is the tensile strength of the axial planar anisotropy and T is the tensile strength in all other orientations. The orientation of fractures with respect to the axial planar surface and the tight macroscopic folding indicates that veins only record a small part of the D_1 deformation that is characterised by intense shortening perpendicular to the orientation of veins.

3. Scanline measurements and methodology

The distribution of 114 (D_1) veins was measured (Fig. 3a) in a typical, continuously exposed, 45-m-long profile (profile 1 hereafter) located in the chlorite zone near Argentiera (Fig. 1). An additional 200 (D_1) veins were measured in nine shorter profiles within homogeneous rock types in the same area. These profiles are combined in Fig. 3(b). The sampling sites were chosen because of the continuous and planar nature of the outcrop and because of the weak intensity of D_2 deformation. The scanline profiles were oriented (towards 060°) perpendicular to the strike of the veins and axial planar foliations. The vein thicknesses and positions, the rock type and the lithological boundaries were recorded to an accuracy of approximately 2 mm and down to a resolution of approximately 1 mm. The spacing between veins was measured from vein centre to vein centre. All measurements were corrected for dip, and hence represent true spacings oriented normal to the vein sets.

The vein spacing distributions in the one-dimensional line samples are characterised here by measuring the spacing population as the cumulative frequency distribution of spaces between adjacent fractures (see Harris et al., 1991). This method is simple and has been shown to be capable of distinguishing between different fracture patterns (see Gillespie et al., 1993) but it is only one of several possible ways of characterising the fracture spacing distribution. Alternative treatments involving interval counting (e.g. Velde et al., 1990), box-counting (e.g. Barton et al., 1993) or fracture density techniques (e.g. La Pointe, 1988) have also been used extensively in the literature. The reader is referred to Barton (1995) for a review and further references on such methodology. The vein thickness distribution is not focussed upon within this paper, but has been characterised in a number of other studies (e.g. see Kruhl, 1994) with the aim of gaining insight into vein forming processes.

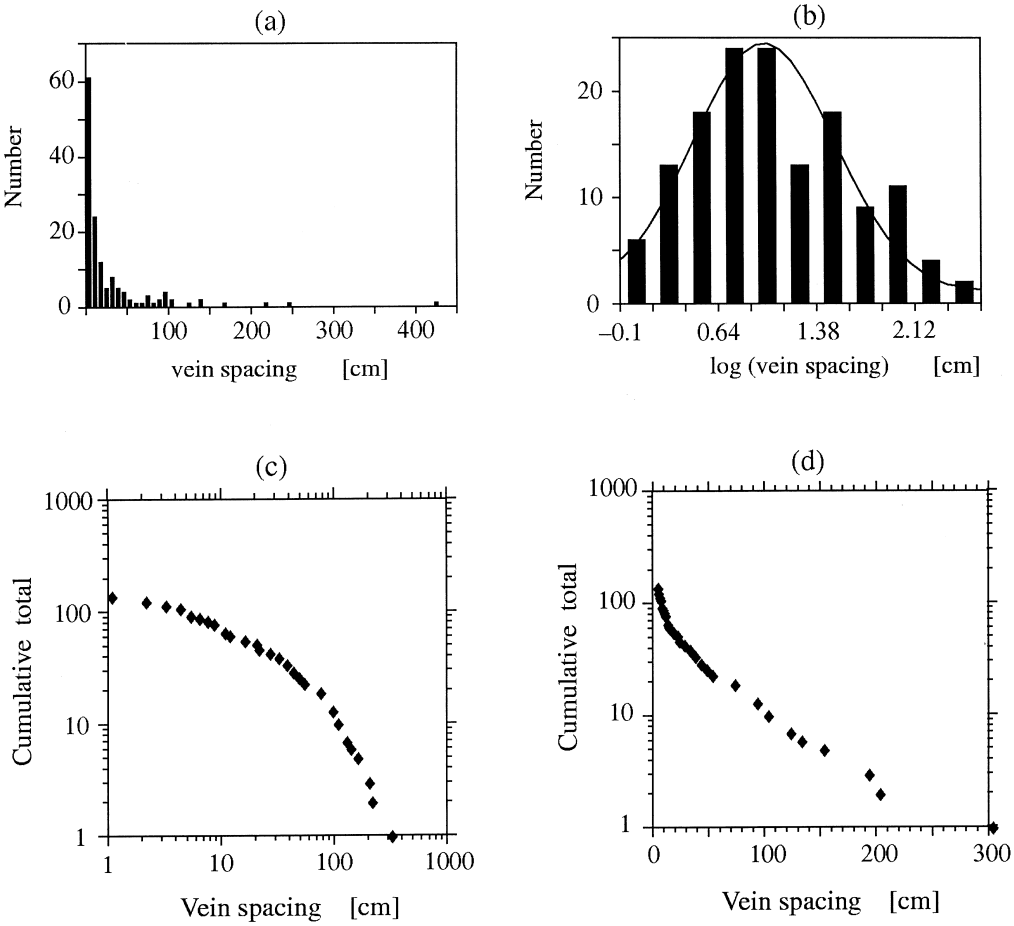

Fig. 4. Measured vein spacing data for profile 1 shown on (a) linear histogram, (b) logarithmic histogram (solid line is the normally distributed fit), (c) plot of logarithmic cumulative frequency versus logarithmic vein, (d) plot of logarithmic cumulative frequency versus linear vein spacing. Power-law distributions plot straight lines on log–log axes (c) whereas negative-exponential distributions plot as straight lines on log–linear axes (d). A Chi-squared test (Table 1) indicates that the vein-spacing distribution is approximated by a log-normal distribution.

4. Results and characterisation of the vein spacing distribution

Three vein spacing distributions have been investigated:

1. Veins in profile 1, regardless of host rock type (Fig. 3a)
2. Veins in psammitic rock types (units B, D and F in Fig. 3b)
3. Veins in pelitic rock types (units A, C, E, G, and I in Fig. 3b)

The vein distributions in psammitic and pelitic rock types were compiled from the eight longest profiles presented in Fig. 3(b) (i.e. excluding section H). The distribution of veins in both measured profiles is irregular (Fig. 3). In profile 1, veining is an order of magnitude more abundant in the pelitic units (14% volume veins) than the psammitic units (1.5% volume veins) and the average vein spacing in pelitic units (18 cm) is almost an order of magnitude smaller than the average vein spacing in the psammitic units (1.3 m). While these observations indicate that the location of veins is strongly influenced by the distribution of rock types, veins within homogeneous rock types also display non-uniform, clustered distributions. This clustering, which is unrelated to rock type variation, is particularly evident in Fig. 3(a) between 37 and 45 m and in Fig. 3(b) between 4.2 and 8.2 m and between 11.3 and 13.5 m. The vein spacing data for profile 1 have a skewed distribution (with a mean vein spacing of 28 cm and a median of 10 cm) on a linear histogram (Fig. 4a) and a reasonably symmetrical distribution on a logarithmic histogram (Fig. 4b). Cumulative frequency–vein spacing plots of this data set are convex-up on log–log axes (Fig. 4c) and convex-down on log–linear axes (Fig. 4d) indicating that the vein spacing distribution is not well described by a power-law nor by a negative exponential, respectively. On the basis of a Chi-squared test (Table 1), the observed vein spacings support the hypothesis (at the 5% level) that the data were drawn from a log-normal population.

The vein spacing distributions (but not their absolute spacings and abundances) in the pelites and psammites are statistically indistinguishable (Fig. 5) and are similar to the distribution of veins in profile 1 (Fig. 4). Both rock types have skewed vein spacing distributions on linear histograms (Fig. 5a and b) and symmetrical distributions on logarithmic histograms (Fig. 5e and f). On cumulative frequency–vein spacing plots both pelites and psammites have distributions which are convex-up on log–log axes (Fig. 5c) and convex-down on log–linear axes (Fig. 5d). Once again, the hypothesis that the data can be described by a log-normal distribution is accepted at the 5% level on the basis of a Chi-squared test (Table 1).

Table 1
Chi-squared tests (Krumbein and Graybill, 1965) of the hypothesis that the vein spacing data were drawn from log-normal populations. N = number of data points, SD = standard deviation, DOF = degrees of freedom, $U = \sum_{i=1}^{n}(N_i - Np_i)^2/Np_i$ (where Np_i is the expected frequency, N_i is the observed frequency, n is the number of intervals (= DOF + 1) and $\chi^2_{0.05}$(DOF) is the Chi-squared value at the 5% level for the relevant degree of freedom). The hypothesis tested can be accepted (i.e. $U < \chi^2_{0.05}$) at the 5% level for all three distributions investigated

	Total profile 1	Psammites	Pelites
N	144	104	88
Mean (log 10)	1.055	0.817	0.823
SD	0.60	0.47	0.47
DOF	11	6	5
U	9.9	0.6	4.4
$\chi^2_{0.05}$(DOF)	18.3	12.6	11.1

5. Discussion

5.1. Influence of heterogeneity in controlling the spacing distribution

The results presented here demonstrate that although the vein abundance and absolute vein spacing is strongly influenced by rock type (Fig. 3), the vein spacing distribution is independent of rock type (cf. Figs. 4 and 5). Thus the origin of the vein spacing distribution is apparently unrelated to the distribution of rock types. Furthermore, the observed log-normal distribution is not controlled by the distribution of the (approximately) uniformly spaced lobe-and-cusp structures, although these structures clearly influence the distribution locally (Fig. 2b). That the lobe-and-cusp structures do not control the vein spacing distribution is also indicated by the fact that the average vein spacing in pelitic (18 cm) and psammitic (1.3 m) rocks for profile 1 are significantly different.

5.2. Influence of deformation on the vein spacing deformation

D_2 deformation is not anticipated to have significantly affected the vein spacing distribution due to its weak intensity in the specifically selected sections (e.g. see Fig. 2a). The influence of D_1 deformation on the vein spacing deformation is, however potentially important although difficult to quantify. The observation of different degrees of boudinage for directly adjacent veins does indicate that veining occurred at different times during the D_1 deformation. One effect that the D_1 deformation is likely to have had on the vein spacing distribution is to reduce the frequency of spaces preferentially at the smallest dimensions. For example, two initially closely spaced axial planar veins may appear as a single vein after deformation involving shortening perpendicular to the veins. Such deformation may cause the modification of a population which initially plots as a power law on a log-spacing versus log-frequency diagram to exhibit 'roll over' at small vein spacing which may then appear non-fractal. Indeed, such a mechanism may be one explanation for the difference between the log-normal spacing distribution described here (see also Fisher et al., 1995) and the fractal distributions described in some other studies (Johnston, 1992; McCaffrey et al., 1993; Manning, 1994). Unfortunately, it is difficult to be more precise about the magnitude of such overprinting effects due to the lack of timing constraints on the timing of the veins relative to each other and with respect to the deformation of the enclosing rocks.

5.3. Implications of the observed spacing distribution

A comparison of the observed vein spacing data with various synthetically generated (one-dimensional) fracture patterns serves as a useful indicator of the types of processes which may have been responsible for controlling the observed distribution (see also Gillespie et al., 1993). To this end, four distributions generated by the following well-known stochastic processes are considered:

1. Regular bisection. This process yields an even distribution with a constant spacing.
2. Random point distribution. Fractures are randomly distributed along the length of a profile, generating a negative exponential distribution (Priest and Hudson, 1976).
3. Kolmogorov fragmentation. This iterative process of random bisection can be simulated by placing two initial fractures at random positions and by successively breaking each fracture-bound segment at a random position (Aitchison and Brown, 1957).
4. A scale invariant, fractal process (the Cantor Dust). A fractal distribution can be generated by breaking

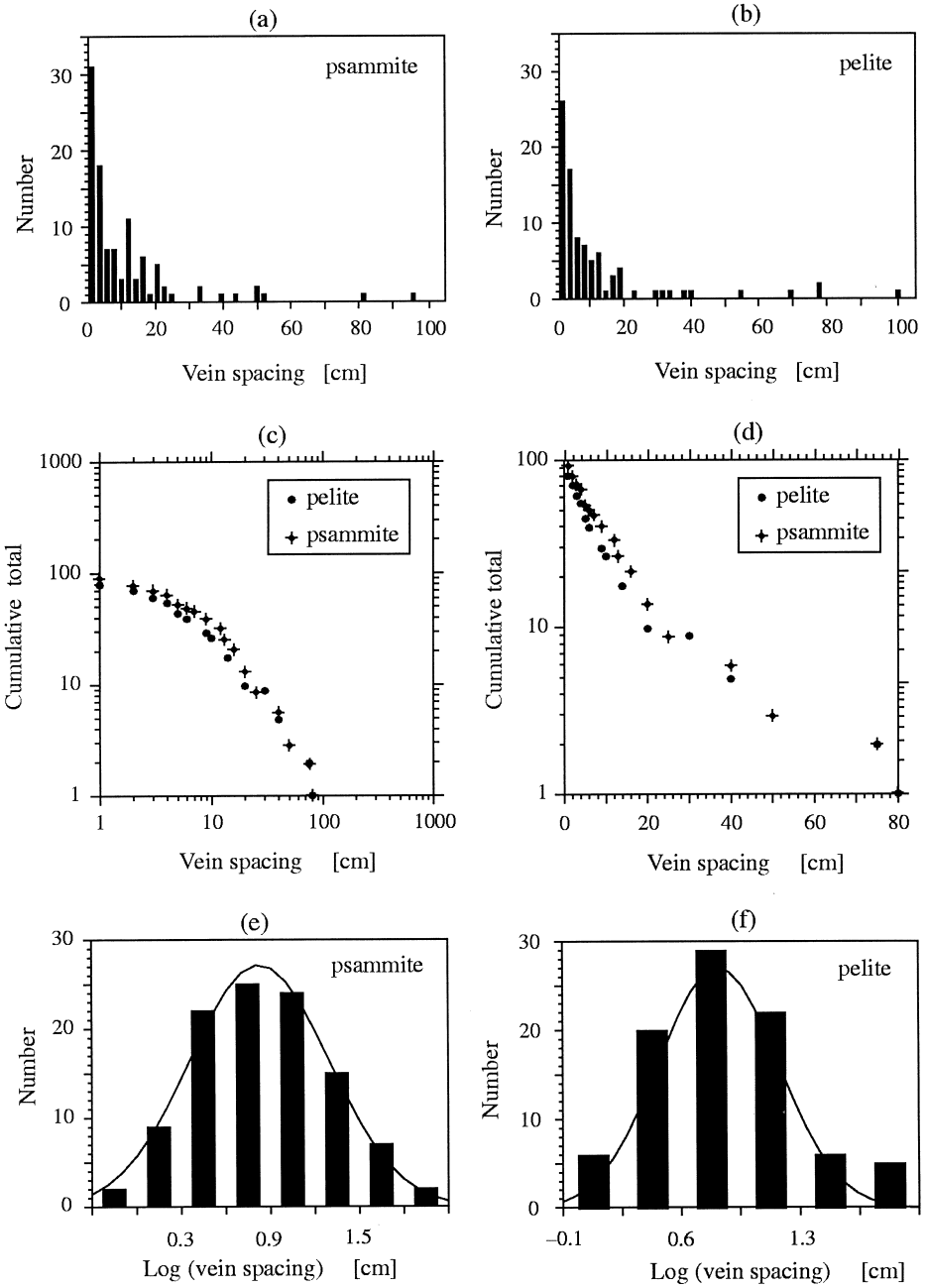

Fig. 5. Vein spacing distributions for the pelitic and psammitic units presented in Fig. 3(b) (excluding the thin psammitic unit labelled H). The data are shown on linear histograms (a and b), logarithmic cumulative frequency versus logarithmic vein-spacing plots (c), logarithmic cumulative frequency versus linear vein-spacing plots (d), and logarithmic histograms (e and f). The solid lines in (e) and (f) show normal distributions fitted to the logarithmic vein-spacing histograms. The vein-spacing populations are statistically indistinguishable in the different rock types and are best approximated by log-normal distributions (Table 1).

the centre third of a profile, and then breaking the centre third of the two remaining segments, and repeating iteratively (Mandelbrot, 1983).

The observed data and theoretical distributions are plotted on a diagram of logarithmic frequency versus logarithmic (inverse) spacing (Fig. 6), which proves useful in comparing and discriminating between different types of distributions (see Chilès, 1988). The Kolmogorov fragmentation process generates a characteristically log-normal fracture spacing distribution (Aitchison and Brown, 1957) that closely matches the observed distribution. The observed vein spacing distribution is not well reproduced by either the random or regular bisection fracture generation processes, both of which lead to fracture patterns less clustered than are actually observed. Likewise, the observed distribution

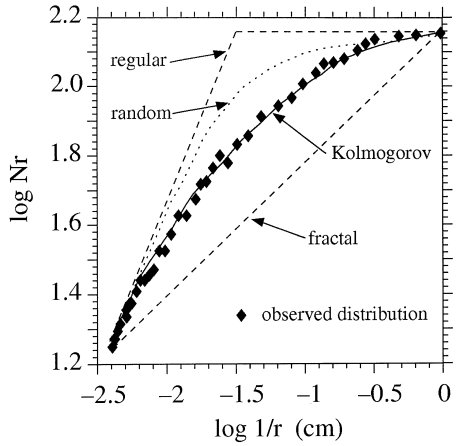

Fig. 6. Comparison between the observed vein-spacing distribution (for profile 1) and various other population distributions (uniform, negative exponential (random), log-normal and fractal) generated by common stochastic processes (see text for discussion). The measured (approximately log-normal) distribution is well reproduced by Kolmogorov fragmentation (curve roughness is a numerical artifact). The plot is obtained by dividing the section into equally spaced subdivisions of length r and counting the number of subdivisions that contain one or more veins, Nr. The range in r that can be investigated is an intrinsic property of the data set and is defined by both upper and lower cut-offs (Chilès, 1988). The upper cut-off is the value of r for which each segment is intersected by at least one vein. The lower cut-off is defined by the width of the veins.

is not well reproduced by the scale invariant Cantor Dust process, which leads to a distribution more clustered than that observed.

The comparison presented in Fig. 6 demonstrates that the observed vein spacing distribution cannot be generated by a random process. In fact, the process leading to the observed distribution must involve interaction between fractures, such as that simulated by the iterative procedure carried out during Kolmogorov fragmentation. It is difficult to determine the significance of the result that the observed distribution is not well reproduced by the fractal process, especially considering the possibility that such a distribution may well have been obliterated by D_1 deformation (see Section 5.2). In addition, a multifractal process or the supposition of different fractal subpopulations may generate distributions closely similar to the observed distribution (see Ranalli and Hardy, 1990). What the comparison with the synthetically generated fracture patterns does indicate is that the observed distribution is similar to the distributions generated by processes involving interactions rather than random uncorrelated behaviour.

5.4. Potential controls on vein spacing

The discussions in Sections 5.1 and 5.3 have shown that the observed vein spacing distribution was controlled by neither heterogeneity nor randomness, but

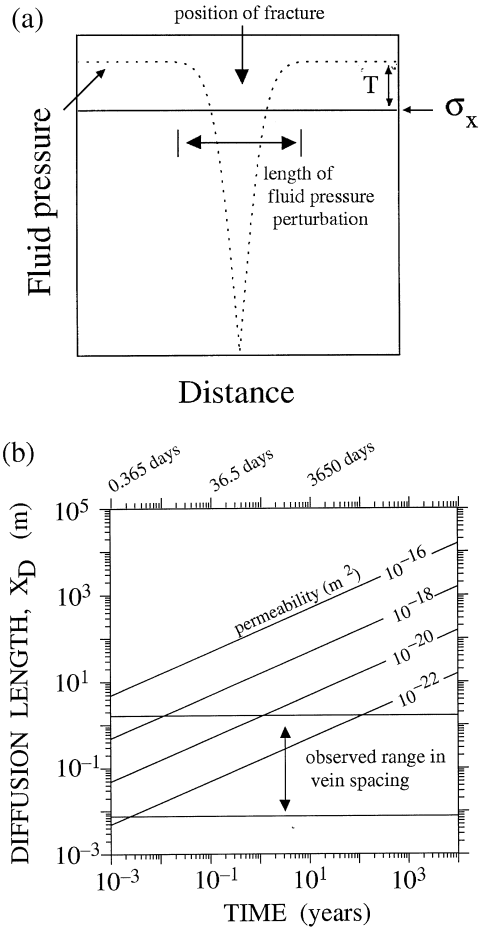

Fig. 7. (a) Schematic diagram (modified after Ladeira and Price, 1981), which illustrates the hypothesis that the perturbation of fluid pressure around an open underpressured hydrofracture may prevent the initiation of new fractures close to an existing fracture (σ_x is the normal stress acting on the surface of a fracture, T is the tensile rock strength). (b) Plot of the characteristic length that a transient in a scalar potential diffuses for a variety of times and permeabilities. Calculated from Eq. (3) using $S_s = 10^{-5}\ m^{-1}$, $\rho_f = 950\ kg\ m^{-3}$, $g = 9.8\ m\ s^{-2}$ and $\mu = 5 \times 10^{-4}\ kg\ m^{-1}\ s^{-1}$. The observed range in vein spacings is also shown.

was influenced by interaction between fractures. This section briefly considers two potential sources for interaction between fractures to investigate whether they can explain the observed non-random distribution. In the following text, it is recognised that although veins represent fractures, the veins themselves reveal no direct information regarding the initiation and evolution of fractures to the observed veins. It is appreciated that each vein may result from more than one fracturing event and that veins may have different ages even though all veins formed within the same episode of deformation.

5.4.1. Fracture-induced perturbation of fluid pressure

Ladeira and Price (1981) suggested a factor which may influence the spacing between hydrofractures

whereby the initiation of a fracture causes a localised zone of reduced fluid pressure to develop, which will tend to inhibit the initiation of new fractures close to the existing open fractures (Fig. 7a). If this mechanism is dominant in the generation of the observed vein spacing distribution, the fracture spacing is predicted to be no smaller than the length scale of the fluid pressure perturbation. An estimation of the characteristic length scale over which the perturbation of fluid pressure propagates by diffusion can be obtained from the relation (e.g. Turcotte and Schubert, 1982, p. 177):

$$X_{\mathrm{D}} = \sqrt{4tD} \tag{3}$$

where X_{D} is the characteristic distance that a transient in a scalar potential diffuses in a time t, and the hydraulic diffusivity D ($\mathrm{m^2\,s^{-1}}$), is:

$$D = \frac{\kappa}{S_{\mathrm{s}}}$$

where κ is the hydraulic conductivity ($= k\rho_{\mathrm{f}}g/\mu$), S_{s} is the specific storage ($\mathrm{m^{-1}}$), k is the permeability ($\mathrm{m^2}$), p_{f} is the fluid density ($\mathrm{kg\,m^{-3}}$), g is the gravitational constant ($\mathrm{m\,s^{-2}}$) and μ is the dynamic fluid viscosity ($\mathrm{kg\,m^{-1}\,s^{-1}}$). Calculations based on this relation (Fig. 7b) show that even for a low permeability of $10^{-20}\,\mathrm{m^2}$, pressure perturbations will equilibrate over length scales of 10 cm in approximately one day. This characteristic diffusion length scale is an order of magnitude greater than the minimum observed vein spacing (ca. 1 cm). This simple consideration indicates that the small veins spacings that are observed are only consistent with the Ladeira and Price (1981) mechanism if permeabilities were less than approximately $10^{-20}\,\mathrm{m^2}$ and if the fracture network developed in a time scale of less than approximately 1 day. More problematic with respect to explaining the observed clustered fracture pattern is the distributed nature of the fracture spacing, which is intuitively anticipated to result from this mechanism.

5.4.2. Fracture-induced perturbation of stress field and fluid pressure

A factor not considered in the above analysis is that in order to maintain mechanical equilibrium, the compressive stress acting on the crack surface must equal the fluid pressure in the crack. This requires that both the fluid pressure and the principal stress trajectories must be perturbed in the vicinity of open fractures. Simple estimates for both stress and fluid pressure perturbations are considered here.

Pollard and Segall (1987) provide analytical solutions for the perturbations of the stress field existing around underpressured open (mode I) fractures embedded in an undeforming elastic media. The one-dimensional perturbation of stress that extends perpendicular to a fracture from midway along its length is described by the relation:

$$\sigma'_x = \frac{\sigma^r_x - \sigma_x}{\sigma^r_x - p_{\mathrm{f}}} = -x^3(x^2 + a^2)^{-3/2} - 1 \tag{4}$$

where σ'_x is the dimensionless stress, σ^r_x is the remote applied normal compressive stress, σ_x is the local normal compressive stress, p_{f} is the fluid pressure in the crack, x is the orthogonal distance from the crack and a is the fracture half-length. The fluid pressure term in Eq. (4) may also be a function of time, space and hydraulic diffusivity. Insight into the characteristic shape and evolution of the fluid pressure perturbation can be obtained by considering the time-dependent analytical solution to the one-dimensional diffusion equation for the decay of a semi-infinite slab confined $-h < x < h$. Assuming no advection and no source or sink, the fluid diffusion equation is:

$$\frac{\mathrm{d}p_{\mathrm{f}}}{\mathrm{d}t} = \kappa\frac{\mathrm{d}^2p_{\mathrm{f}}}{\mathrm{d}x^2}, \tag{5}$$

the solution of which is (Carslaw and Jaeger, 1959, p. 54):

$$p'_{\mathrm{f}} = \frac{p^r_{\mathrm{f}} - p_{\mathrm{f}}}{p^r_{\mathrm{f}} - p^0_{\mathrm{f}}} = \frac{1}{2}\left(\mathrm{erf}\frac{h-x}{2\sqrt{Dt}} + \mathrm{erf}\frac{h+x}{2\sqrt{Dt}}\right) \tag{6}$$

where p'_{f} is the dimensionless fluid pressure, p^r_{f} is the initial fluid pressure in the rock, p^0_{f} is the initial fluid pressure in the fracture, D is the hydraulic diffusivity, κ is the hydraulic conductivity and t is the time. The calculated stress and fluid pressure perturbations associated with an underpressured hydrofracture obtained by combining Eqs. (4) and (6) are presented in Fig. 8.

Fig. 8 illustrates that the initiation of an isolated, underpressured fracture instantaneously generates a zone, initially extending laterally over a length scale of approximately two fracture lengths either side of the fracture, which satisfies the failure condition for the formation of new fractures (i.e. $p'_{\mathrm{f}} > \sigma'_x + T$). This critically stressed zone is predicted to be a site for the preferential nucleation of new fractures, the positions of which are anticipated to be variable dependent on a number of factors including the position relative to the adjacent fractures, time, diffusivity, fracture length and local heterogeneity. Such a mechanism is predicted to lead to the formation of clustered fracture distributions which have no lower limit to the fracture spacing. This mechanism will operate regardless of the characteristic diffusion length since the critically stressed zone is created instantaneously.

5.4.3. Numerical simulation of localising mechanism

A simple one-dimensional discrete numerical model

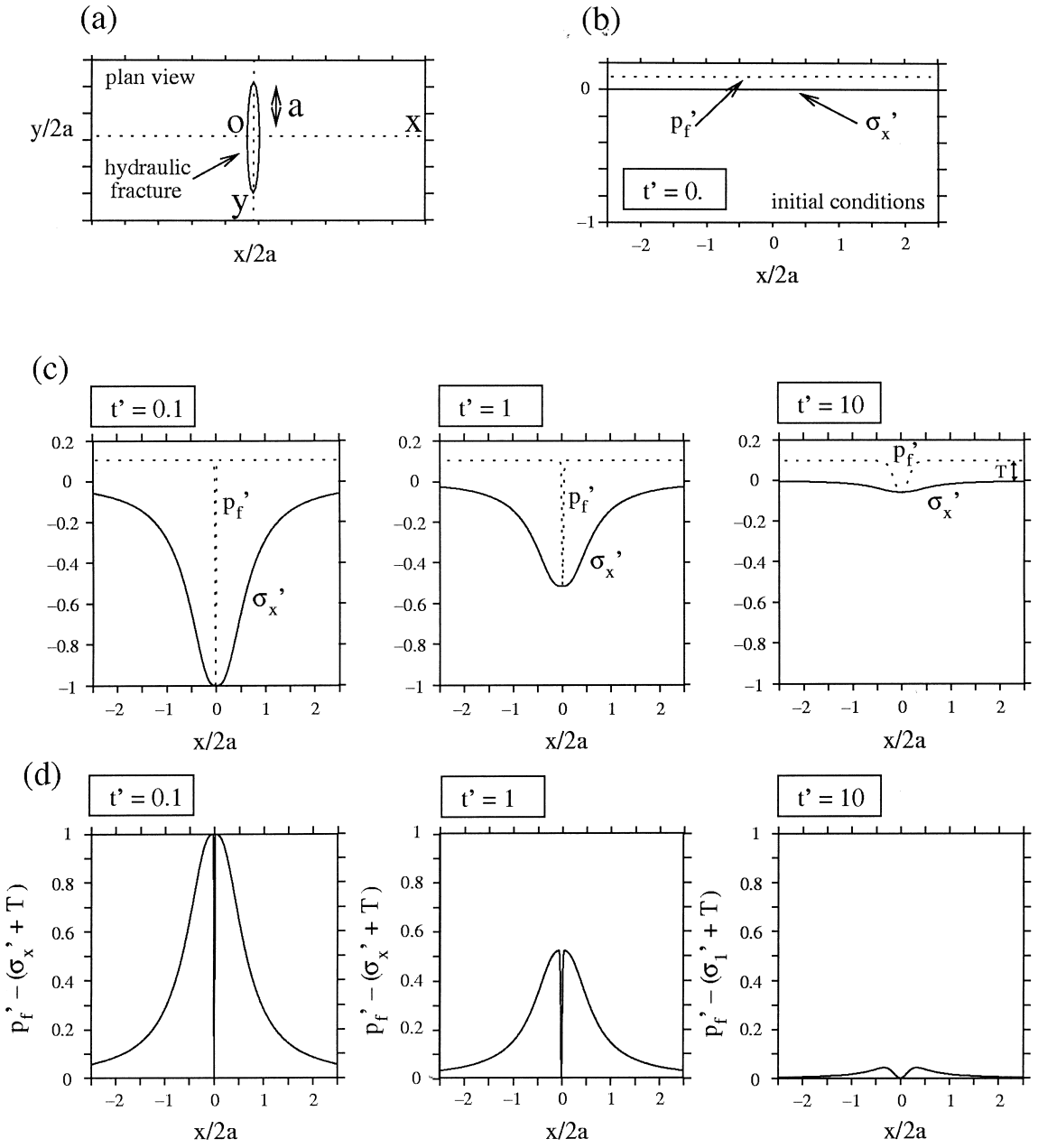

Fig. 8. Calculated perturbations of the fluid pressure, normal stress and effective pressure in a one-dimensional profile oriented perpendicular to and midway along an open underpressured hydraulic fracture of length $2a$. The two upper diagrams show the reference frame in plan view (a) and the initial conditions (b) for the fluid pressure and normal stress along the profile in the x direction. (c) Plot of distance $(x/2a)$ versus fluid pressure $(p_f' = (p_f^r - p_f)/(p_f^r - p_f^0))$ and normal stress $(\sigma_x' = (\sigma_x^r - \sigma_x)/(\sigma_x^r - p_f))$ for three different times $(t' = \sqrt{Dt/h^2})$, where p_f^r is the initial fluid pressure in the rock, p_f^0 is the initial fluid pressure in the fracture, D is the hydraulic diffusivity and t is the time. The fluid pressure prior to failure (0.1) is uniformly equal to $\sigma_x' + T$, where T is the tensile strength. (d) Plot of the distance $(x/2a)$ versus the effective tensile stress $(p_f' - \sigma_x' + T)$ for three different times. Note that the failure condition is satisfied wherever the plotted value of the tensile effective stress exceeds zero. The fluid pressure profile is the time-dependent analytical solution (Eq. 6) to the one-dimensional fluid diffusion equation $(h/2a = 0.01)$. This solution strictly applies to a semi-infinite sink (i.e. $2a \rightarrow \infty$) and hence should be viewed as schematic. The stress profile was calculated from Eq. (4) after Pollard and Segall (1987).

was developed in order to determine the nature of the fracture spacing distribution generated by the potential interaction between stress and fluid perturbations associated with hydrofracturing. Initial conditions applied to a calculation domain consisting of 5000 regularly spaced intervals comprise (1) constant initial normal stress $(\sigma_x = \sigma_x^r)$, (2) tensile strength T_i specified to vary randomly between 0 and T, and (3) initial fluid pressure $(p_f = p_f^r = p_f^0)$ that everywhere satisfies the condition for hydrofracture (i.e. $p_f = \sigma_x + T_i$).

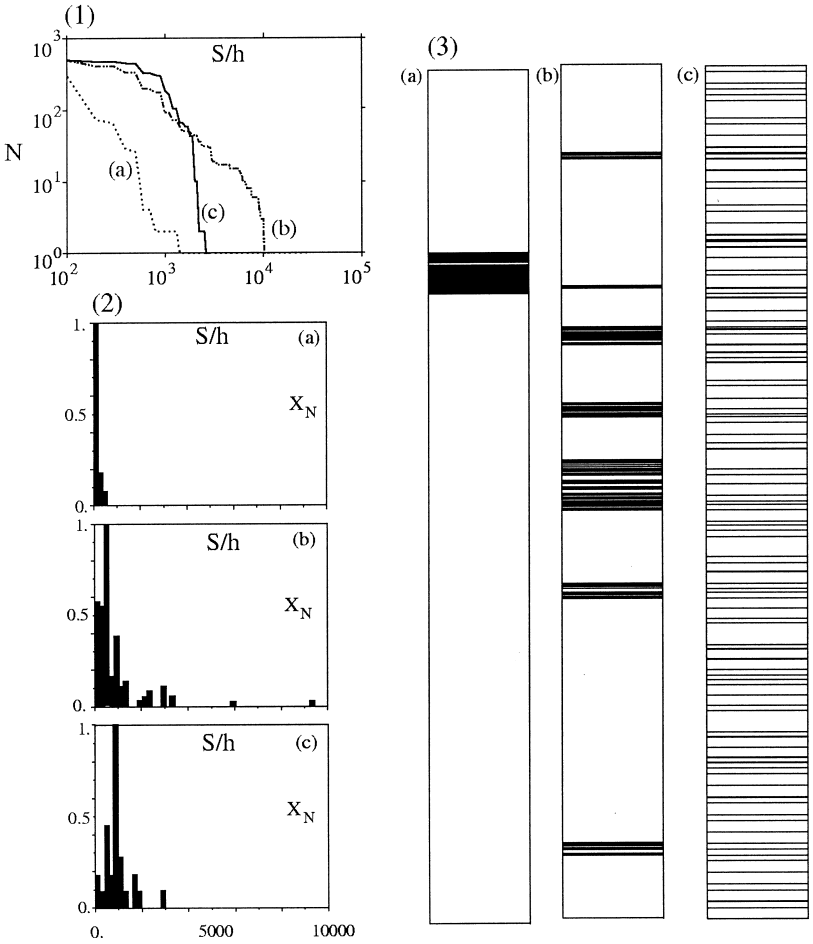

Fig. 9. Numerical results illustrating the effect that hydraulic fracture-induced perturbations of the fluid pressure and stress may have on the subsequent fracture spacing distribution. The formation of 500 hydraulic fractures was simulated (as governed by Eqs.1, 4 and 6) in a simple one-dimensional model (see text for explanation) as a function of three parameters, dimensionless stress ($s' = (\sigma_x^r + T)/p_f^0 = 10$), dimensionless length (calculated with $l' = a/h = 1000$) and dimensionless time ($t' = \sqrt{(Dt)/h^2}$). The results of three simulations (labelled a, b, c) are reported on plots of (1) log-cumulative frequency (N) versus normalised log-spacing (where S is the fracture spacing and h is the fracture half width), (2) linear histograms (S/h versus X_N where X_N is the proportion of the total fracture population) and (3) fracture transects (a: $t' = 2.34$; b: $t' = 4.26$; c: $t' = 10.0$).

Fracturing is initiated by instantaneously dropping the fluid pressure by a fixed amount (to a value below σ_x^r) at a single node chosen at random. After calculating the perturbation of both the fluid and the stress resulting from the presence of the fracture (using Eqs. 4 and 6), the calculation domain is searched for the node with the greatest tensile effective stress exceeding the failure condition, which is chosen as the next position for failure. This procedure is repeated until the desired number of fracture events (typically 500) has taken place. The fluid and stress perturbations resulting from previous failure events are retained cumulatively throughout the calculation so that these events influence a control on the location of future fractures.

Synthetic fracture spacing distributions were simulated as a function of three parameters: dimensionless stress ($s' = (\sigma_x^r + T)/p_f^0$), dimensionless length ($l' = a/h$) and dimensionless time ($t' = \sqrt{(Dt)/h^2}$) (the symbols have the same meaning as those defined above). Results of three simulations for different values of t', (labelled a, b, c) which illustrate the full range of model behaviour observed, are presented in Fig. 9. For small values of t' (short intervals of time and/or low permeabilities) the entire fracture spacing distribution is localised in the close vicinity of the initial fracture (Fig. 9a) due to creation of large tensile effective stresses exceeding the failure condition (see also Fig. 8). As t' is increased the magnitude of the tensile effective stresses created by fracture events decreases and the heterogeneity introduced by randomness in the tensile strength has an increasingly important effect in controlling the location of new fractures. The result is the transition to a spacing distribution which is characteristically positively skewed and exhibits a large range in fracture spacings (Fig. 9b) and eventually to a distribution which is controlled entirely by randomness

(Fig. 9c). Increasing l' (i.e. increasing the fracture length and therefore the range of stress perturbation) and increasing s' (i.e. increasing the stress drop associated with fracturing) have the same (though less dramatic) effects as decreasing t'.

In the model simulations, the fracture spacing distribution is controlled by the trade-off between system-inherent features (i.e. randomness introduced in the tensile rock strength) which act to homogenise the distribution, and process-inherent features (stress and fluid pressure perturbations created by fracture) which, in this case, are strongly localising. The transition between these two end-member regimes is a function of time, permeability, the crack aspect ratio and the stress drop in the fracture. The simulations demonstrate some of the complexity that may be involved in the formation of fracture distributions and in particular, the potential for a single simple process to give rise to a variety of distributions which evolve as a function of time (Fig. 9). This complexity may well be important in explaining the variety of vein spacing distributions, that have already been described in the literature (see Johnston, 1992; McCaffrey et al., 1993; Manning, 1994; Fisher et al., 1995). The instability created by the initial hydraulic fracture is limited by the ability of fractures to remain underpressured with respect to the remote normal stress. This instability would not occur if the formed fractures immediately closed or if the fluid pressure in fractures remained at the magnitude of the remote normal stress.

Even though it is difficult to relate the results of the simple model to the observed vein spacing distributions, simulation (b) does share similarities with respect to the form of the observed data when plotted on a log-cumulative frequency versus log-spacing diagram (cf. Figs. 9.1b and 4c) and on a histogram (cf. Figs. 9.2b and 4a). That the fracture spacing distribution of this simulation (i.e. b) is controlled by important degrees of both heterogeneity and interaction between fractures is also consistent with field observations, which show that some veining is controlled by heterogeneities (Fig. 2b), but that there is also clustering unrelated to structures existing in the rock (see Section 4).

Although the model presented here is able to reproduce some features consistent with the observed vein spacing distribution, the model and the proposed localising mechanism are limited by their simplicity. Both stress and fluid pressure distributions around fractures are known to be more complex than implied by Eqs. (4) and (6), and to exhibit features which cannot be adequately accounted for in a one-dimensional analysis. Likewise, neither of Eqs. (4) and (6) are strictly applicable to the situation modelled here where fractures are closely spaced and strongly interacting. More realistic models could be developed to overcome these difficulties and to provide a more rigorous test of the proposed localising mechanism.

6. Summary and conclusions

Synmetamorphic axial planar veins measured in greenschist facies meta-sediments exposed on NW Sardinia display a non-uniform spacing distribution, which is best described as log-normal. Although the vein abundance and absolute vein spacing is strongly influenced by rock type, the vein spacing distribution is independent of rock type. Thus the origin of the vein spacing distribution is unrelated to the distribution of rock types. Comparison of the observed spacing distribution with synthetically generated fracture distributions indicates that the observed distribution can be reproduced by the process defined by Kolmogorov fragmentation but cannot be reproduced by a random or even-bisection process. These results indicate that the positions of the fractures that formed the veins are interdependent, in that once a fracture is initiated, this fracture influences where subsequent fractures will initiate. The observed vein spacing is, however, significantly less clustered than predicted by a fractal (Cantor Dust) process.

To determine potential mechanisms by which the position of fractures (veins) may be interdependent, the perturbations of stress and fluid pressure associated with an isolated open underpressured hydrofracture were investigated. Simple calculations show that the fluid pressure drop inside a fracture coinciding with failure creates a zone in the surrounding rock, extending over a lateral extent equivalent to approximately two fracture lengths, which is instantaneously driven into a critical stress state that satisfies the failure condition. Results of a simple numerical model demonstrate that this process will tend to localise the nucleation of subsequent fractures close to existing fractures, leading to a non-random or clustered spacing distribution.

Acknowledgements

I am grateful to A. Thompson, J. Connolly, J. Ridley and Y. Podladchikov for constructive discussions and for reading drafts of this manuscript. The paper has also benefitted greatly due to the reviews of J. H. Kruhl and K. McCaffrey and to the comments and suggestions of the associate editor T. G. Blenkinsop. I acknowledge V. Trommsdorf for suggesting the study area and thank B. Mountain for providing field assistance. This project was funded by ETH-Forschungsproject 0-20-885-94.

References

Aitchison, J., Brown, J.A.C., 1957. The Lognormal Distribution. Cambridge University Press, Cambridge 176 pp.

Barton, C.C., Larsen, E., Page, W.R., Howard, T.M., 1993. Characterising fractured rock for fluid flow, geomechanical, and paleostress modelling: methods and preliminary results from Yucca Mountain, Nevada (Methods for parameterizing fracture characteristics at the scale of large outcrops), U.S. Geological Survey Open File report 93-0269.

Barton, C.C., 1995. Fractal analysis of scaling and spatial clustering of fractures. In: Barton, C.C., La Pointe, P.R. (Eds.), Fractals in the Earth Sciences. Plenum Press, New York, pp. 141–178.

Blenkinsop, T.G., 1993. Fracture spacing distributions in rock. International Symposium on Fractals and Dynamic Systems in Geoscience, Book of Abstracts. Johann Wolfgang Goethe-University, Frankfurt am Main, Germany, 1–3 April.

Carmignani, L., Franceschelli, M., Pertsati, P.C., Memmi, I., Ricci, C.A., 1979. Evoluzione tettonico-metamorphica del basamento ercinico della Nurra (Sardegna, NW). Memorie della Società Geologica Italiana 20, 57–84.

Carmignani, L., Franceschelli, M., Memmi, I., Ricci, C.A., 1982. An example of compositional control on the celadonitic content of muscovite and the incoming of biotite in metapelites (Nurra, NW Sardinia). Neues Jahrbuch für Mineralogie, Monatshefte 7, 389–401.

Carslaw, H.S., Jaeger, J.C., 1959. Conduction of Heat in Solids, 2nd ed. Oxford University Press, London 510 pp.

Cartwright, I., Power, W.L., Oliver, N.H.S., Valenta, R.K., McLatchie, G.S., 1994. Fluid migration and vein formation during deformation and greenschist facies metamorphism at Oriston Gorge, central Australia. Journal of Metamorphic Geology 12, 373–386.

Chilès, J.P., 1988. Fractal and geostatistical methods for modelling of a fracture network. Mathematical Geology 20, 631–654.

Fisher, D.M., Brantley, S.L., Everett, M., Dzonik, J., 1995. Cyclic fluid flow through a regionally extensive fracture network within the Kodiac accretionary prism. Journal of Geophysical Research 100, 12881–12894.

Fisher, D.M., Byrne, T., 1990. The character and distribution of mineralised fractures in the Kodiak Formation, Alaska: implications for fluid flow in an underthrust sequence. Journal of Geophysical Research 95, 9069–9080.

Franceschelli, M., Pannuti, F., Puxeddu, M., 1990. Texture development and PT time path of psammitic schist from the Hercynian chain of NW Sardinia (Italy). European Journal of Mineralogy 2, 385–398.

Gillespie, P.A., Howard, C.B., Walsh, J.J., Watterson, J., 1993. Measurement and characterisation of spatial distribution of fractures. Tectonophysics 226, 113–141.

Gratier, J.P., 1987. Pressure solution-deposition creep and the associated tectonic differentiation in sedimentary rocks. In: Jones, M.E., Preston, R.M.F. (Eds.), Deformation of Sediments and Sedimentary Rocks, Special Publication of the Geological Society of London, pp. 25–38.

Harris, C., Franssen, R., Loosveld, R., 1991. Fractal analysis of fractures in rocks: the Cantor's Dust method—comment. Tectonophysics 198, 107–115.

Johnston, J.D., 1992. The fractal geometry of vein systems—potential for ore reserve calculation. In: Earls, A., Bowden, A., Pyne, J., O'Connor, P. (Eds.), The Irish minerals industry—a review of the decade, Galway 1990. Irish Association for Economic Geology, Dublin, pp. 105–117.

Kerrich, R., 1986. Fluid infiltration into fault zones: chemical, isotropic and mechanical effects. Pure and Applied Geophysics 124, 225–268.

Kruhl, J.H., 1994. The formation of extensional veins: An application of the Cantor-Dust model. In: Kruhl, J.H. (Ed.), Fractals and Dynamic Systems in Geoscience. Springer-Verlag, Berlin, pp. 95–104.

Krumbein, W.C., Graybill, F.A., 1965. An Introduction to Statistical Models in Geology. McGraw-Hill, New York 476 pp.

Ladeira, F.L., Price, N.J., 1981. Relationship between fracture spacing and bed thickness. Journal of Structural Geology 3, 179–183.

La Pointe, P.R., 1988. A method to characterise fracture density and connectivity through fractal geometry. International Journal of Rock Mechanics and Mining Science, Geomechanical Abstracts 25, 421–429.

Mandelbrot, B.B., 1983. The fractal Geometry of Nature. Freeman, New York 468 pp.

Manning, C.E., 1994. Fractal clustering of metamorphic veins. Geology 22, 335–338.

McCaffrey, K., Johnston, D., Feely, M., 1993. Use of fractal statistics in the analysis of Mo–Cu mineralisation at Mace Head, County Galway. Irish Journal of Earth Sciences 12, 139–148.

Pollard, D.D., Segall, R., 1987. Theoretical displacements and stresses near fractures in rock: with applications to faults, joints, veins, dikes, and solution surfaces. In: Atkinson, B.K. (Ed.), Fracture Mechanics of Rock, pp. 277–347.

Priest, S.D., Hudson, J.A., 1976. Discontinuity spacing in rock. International Journal of Rock Mechanics and Mining Sciences and Geomechanical Abstracts 13, 135–148.

Ramberg, H., 1961. A study of veins in Caledonian Rocks around Trondheim Fjord, Norway. Norsk Geologisk Tidsskrift 41, 24–43.

Ranalli, G., Hardy, L., 1990. Statistical approach to brittle fracture in the Earth's crust. In: Agterberg, F.P., Bonham-Carter, G.F. (Eds.), Statistical Applications in the Earth Sciences, Geological Survey of Canada Paper, 89-9, pp. 255–262.

Sawyer, E.W., Robin, P.-Y.F., 1986. The subsolidus segregation of layer-parallel quartz–feldspar veins in greenschist to upper amphibolite facies metasediments. Journal of Metamorphic Geology 4, 237–260.

Segall, P., 1984. Formation and growth of extensional fracture sets. Geological Society of America Bulletin 95, 454–462.

Simpson, G.D.H., 1998. Dehydration-related deformation during regional metamorphism, NW Sardinia, Italy. Journal of Metamorphic Geology 16, 457–472.

Turcotte, D.L., Schubert, G., 1982. Geodynamics. Applications of continuum physics to geological problems. John Wiley, New York 450 pp.

Turner, F.J., 1941. The development of pseudostratification by metamorphic differentiation in the schists of Otago, New Zealand. American Journal of Science 239, 1–16.

Velde, B., Dubois, J., Touchard, G., Badri, A., 1990. Fractal analysis of fractures in rocks. Tectonophysics 179, 345–352.

Vidale, R.J., 1974. Vein assemblages and metamorphism in Dutchess County, New York. Geological Society of America Bulletin 85, 303–306.

Voll, G., 1960. New work on petrofabrics. Liverpool and Manchester Geological Journal 2/3, 503–567.

Yardley, B.W.D., 1975. On some quartz–plagioclase veins in the Connemara schists, Ireland. Geological Magazine 112, 183–190.

Yardley, B.W.D., 1986. Fluid migration and veining in the Connemara schists. In: Walther, J.V., Wood, B.J. (Eds.), Fluid–Rock Interactions During Metamorphism. Springer-Verlag, New York, pp. 109–131.

Yardley, B.W.D., Bottrell, S.H., 1992. Silica mobility and fluid movement during metamorphism of the Connemara schists, Ireland. Journal of Metamorphic Geology 10, 453–464.